

**Universidade Federal de São Carlos**  
**Centro de Ciências Exatas e de Tecnologia**  
**Departamento de Engenharia de Materiais**

**Design of a solid-state hydrogen storage tank for application in the  
European Spallation Source (ESS)**

**Gabriela Chimello Mayer Dias**

**São Carlos - SP**

**2021**

# **Design of a solid-state hydrogen storage tank for application in the European Spallation Source (ESS)**

Trabalho de conclusão de curso apresentado ao Departamento de Engenharia de Materiais da Universidade Federal de São Carlos, como requisito para obtenção do título de bacharel em Engenharia de Materiais.

Orientador: Guilherme Zepon

Coorientador: Marcelo Juni Ferreira

São Carlos-SP

2021



## ATA DE DEFESA DE TRABALHO DE CONCLUSÃO DE CURSO (TCC)

**NOME:** Gabriela Chimello Mayer Dias

**RA:** 744385

**TÍTULO:** Design of a solid-state hydrogen storage tank for application in the European Spallation Source (ESS)

**ORIENTADOR(A):** Prof. Dr. Guilherme Zepon

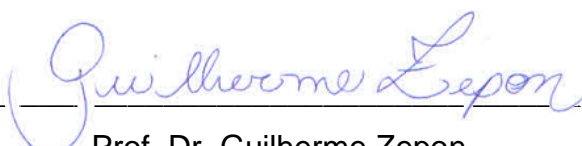
**CO-ORIENTADOR(A):** Dr. Marcelo Juni Ferreira

**DATA/HORÁRIO:** 16/11/2021, 17h

### BANCA – NOTAS:

	Monografia	Defesa
Prof. Dr. Guilherme Zepon	10	10
Prof. Dr. Daniel Rodrigo Leiva	10	10
<b>Média</b>	10	10

Certifico que a defesa de monografia de TCC realizou-se com a participação a distância dos membros Prof. Dr. Guilherme Zepon e Prof. Dr. Daniel Rodrigo Leiva e depois das arguições e deliberações realizadas, os participantes à distância estão de acordo com as informações redigidas nesta ata de defesa.

  
\_\_\_\_\_  
Prof. Dr. Guilherme Zepon

## **Acknowledgments**

First, I would like to thank my supervisor, Guilherme Zepon, for all the support and help to carry out this work. He is undoubtedly an inspiration to me and has guided me throughout my fantastic journey in research during my university years.

I would also like to thank my co-supervisor, Marcelo Juni Ferreira, for the essential guidance and the unique opportunity to do this work correlated with the European Spallation Source.

I am deeply grateful to my parents and my sister for all their love and support, I have no words to describe how important they were for me to get here and be strong and inspired to pursue my dreams.

I am also very grateful to my friends, who were by my side in the last years and during the execution of this work. In special, I would like to thank Fernanda, my best friend and biggest partner in all my journey at the university, and for sure, she was my most significant support during my years in São Carlos.

## Abstract

The European Spallation Source, located in Lund, Sweden, is one of the largest scientific and technological infrastructures currently under construction and will be the world's most powerful neutron source. Its operation will be based on proton acceleration and scattering technology, giving rise to neutron beams up to 100 times brighter than those obtained by existing sources in Europe. In summary, a proton beam is produced by rapidly varying electromagnetic fields, heating hydrogen gas so that electrons evaporate from the hydrogen molecules. The beam will then be accelerated until it hits a target made of stainless steel and containing bricks of tungsten, generating scattering neutrons used in various scientific instruments. However, there is a problem related to the storage of the hydrogen gas used in producing the proton beam. Initially, a cylinder containing 5 liters of H<sub>2</sub> at 150 bar pressure was designed, but local regulations state that the pressure cannot exceed 1.45 bar. In this scenario, hydrogen storage in the solid state through metal hydrides would be an excellent alternative for storing the required volume of hydrogen at a much lower pressure level and with a higher volumetric density. Therefore, the goal of this work was to design a tank for solid-state hydrogen storage, ensuring a pressure level below 1.45 bar. For this, a multicomponent alloy was selected through results reported in the literature and compositional adjustments based on a thermodynamic model that allows the prediction of PCT (Pressure-Composition-Temperature) diagrams. Furthermore, calculations were performed for the tank sizing, and its components were selected and analyzed, resulting in two project options. Next, a cost projection for the tank production was elaborated, involving the costs of raw materials to produce the selected alloy and the components chosen to compose the tank. Finally, a prototype and proof-of-concept tests were proposed to verify essential properties for this project, such as the H<sub>2</sub> flow rate reached.

**Keywords:** Hydrogen solid-state storage; Metal Hydrides; Multicomponent Alloys; Hydrogen Tank.

## Resumo

A European Spallation Source, localizada em Lund, na Suécia, é uma das maiores infraestruturas científicas e tecnológicas em construção atualmente, e será a fonte de nêutrons mais potente do mundo. Seu funcionamento irá se basear na aceleração de prótons e espalhamento, dando origem a feixes de nêutrons 100 vezes mais brilhantes do que os obtidos pelas fontes já existentes na Europa. Basicamente, um feixe de prótons é produzido pelo aquecimento de gás hidrogênio com a variação rápida de campos eletromagnéticos, levando à evaporação dos elétrons das moléculas. Assim, o feixe será acelerado até atingir um alvo de aço inoxidável revestido com tungstênio, gerando o espalhamento de nêutrons que serão utilizados em diversos instrumentos científicos. Entretanto, há um problema relacionado ao armazenamento do gás hidrogênio utilizado na produção do feixe de prótons. De início, foi projetado um cilindro contendo 5 litros de H<sub>2</sub> em 150 bar de pressão, mas a regulamentação local estabelece que a pressão não pode ultrapassar 1,45 bar. Nesse cenário, o armazenamento de hidrogênio no estado sólido por meio de hidretos metálicos seria uma ótima alternativa para a armazenagem do volume requerido de hidrogênio em um nível de pressão muito menor e com uma maior densidade volumétrica. O objetivo deste trabalho de conclusão de curso foi projetar um tanque para a armazenagem de hidrogênio no estado sólido assegurando um nível de pressão abaixo de 1,45 bar. Para isso, uma liga multicomponente foi selecionada através de resultados reportados na literatura e ajustes composicionais baseados em um modelo termodinâmico que permite a previsão de curvas PCT (Pressão-Composição-Temperatura). Ademais, foram realizados cálculos para o dimensionamento do tanque e seus componentes foram selecionados e analisados, resultando em duas opções de projeto. Em seguida, foi elaborada uma projeção dos custos para a produção do tanque, envolvendo os custos das matérias-primas para a produção da liga selecionada e dos componentes escolhidos para compor o tanque. Por fim, um protótipo e testes de prova de conceito foram propostos a fim de verificar propriedades importantes para o projeto, como o fluxo de H<sub>2</sub> obtido.

**Palavras-chave:** Armazenagem de hidrogênio no estado sólido; Hidretos Metálicos; Ligas multicomponentes; Tanque de Hidrogênio.

## Index

1. Introduction and Theoretical Fundamentals.....	10
2. Problem Statement.....	13
3. Material selection.....	13
4. Tank sizing .....	19
4.1 Alloy's mass calculation .....	19
4.2 Alloy's volume calculation .....	20
5. Tank project.....	21
5.1 Components detailing .....	23
5.2 Procedure after the hydrogen depletion.....	27
6. Cost projection.....	29
6.1 (TiVNb) <sub>67</sub> Cr <sub>33</sub> synthesis.....	29
6.2 Tank components .....	30
7. Proposal of a prototype and proof-of-concept tests .....	31
7.1 Prototype description .....	31
7.2 Alloy's synthesis and chemical composition verification .....	32
7.3 PCI diagram measurement .....	32
7.4 Evaluation of the H <sub>2</sub> flow .....	33
7.5 Hydride safety in air contact.....	34
8. Conclusions.....	34
9. References .....	35

## Figure index

<b>Figure 1:</b> Aerial view of the ESS facility (January 2021). Image: Perry Nordeng/ESS. .....	10
<b>Figure 2:</b> Pressure-composition isotherms for a hypothetical metal-hydrogen system.....	12
<b>Figure 3:</b> Schematic pressure-composition isotherms hysteresis.....	12
<b>Figure 4:</b> PCI absorption/desorption isotherms at 24°C. [7] .....	15
<b>Figure 5:</b> Comparison between experimental and calculated PCI diagrams of (TiVNb) <sub>85</sub> Cr <sub>15</sub> [8] .....	16
<b>Figure 6:</b> PCI diagram calculated for the (TiVNb) <sub>65</sub> Cr <sub>35</sub> alloy. ....	17
<b>Figure 7:</b> PCI diagram calculated for five different compositions at 15°C.....	18
<b>Figure 8:</b> PCI diagram calculated for five different compositions at 25°C.....	18
<b>Figure 9:</b> PCT diagram of (TiVNb) <sub>67</sub> Cr <sub>33</sub> at 15°C obtained by the thermodynamic model. ....	20
<b>Figure 10:</b> 3D drawing of project A, with two sample cylinders of 500cm <sup>3</sup> . ....	22
<b>Figure 11:</b> 3D drawing of project B, with five sample cylinders of 150cm <sup>3</sup> . ....	23
<b>Figure 12:</b> Sample cylinders specifications. ....	24
<b>Figure 13:</b> Plug in carbon steel specifications. ....	24
<b>Figure 14:</b> VCR components specifications – female nut, gland, and gasket.....	25
<b>Figure 15:</b> VCR bodies specifications – cross, tee, and elbow.....	25
<b>Figure 16:</b> Valves specifications – needle valve and ball valve .....	26
<b>Figure 17:</b> Female connector (NPT/VCR) body specification.....	26
<b>Figure 18:</b> Seamless tubing specifications. ....	27
<b>Figure 19:</b> Hydrogen absorption capacity in wt% of (TiVNb) <sub>85</sub> Cr <sub>15</sub> , (TiVNb) <sub>95.3</sub> Co <sub>4.7</sub> , and (TiVNb) <sub>96.2</sub> Ni <sub>3.8</sub> alloys as a function of cycles of absorption and desorption.[6] .	28
<b>Figure 20:</b> Sievert's apparatus scheme.....	32



## Table index

<b>Table 1:</b> Plateau pressures at 15°C and 25°C for all the analyzed compositions. ...	19
<b>Table 2:</b> Pure metals specifications – titanium, niobium, vanadium, and chromium	29
<b>Table 3:</b> Required mass, price per gram, and the total price of each pure element.	29
<b>Table 4:</b> Unit prices and the required quantities of each tank component. ....	30

## 1. Introduction and Theoretical Fundamentals

The European Spallation Source (ESS) is a multi-disciplinary research facility under construction in Lund, southern Sweden. It is one of the most significant science and technology infrastructure projects being built today. It will be the world's most powerful neutron source, allowing a breakthrough in scientific discovery in several fields of knowledge, such as materials, fundamental physics, and energy.



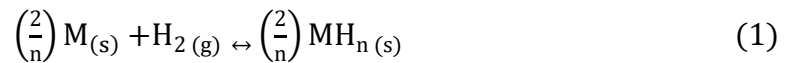
**Figure 1:** Aerial view of the ESS facility (January 2021). Image: Perry Nordeng/ESS.

Unlike the existing neutron sources in Europe, which are based on nuclear reactors, ESS's neutron source is based on particle accelerators and spallation technology, providing up to 100 times brighter neutron beams. In summary, a proton beam is produced by rapidly varying electromagnetic fields, heating hydrogen gas so that electrons evaporate from the hydrogen molecules. The proton beam is guided from the ion source through the accelerator beam line under vacuum, with accelerating structures and beam pipes, until the protons reach 96% of the speed of light. Afterward, the speeded-up proton beam hits a target with 2.6 m of diameter made of stainless steel and containing bricks of tungsten, a neutron-rich heavy metal. The collision of protons and the target's nuclei scatters high-energy neutrons, which are slowed down from 10% of the speed of light to approximately the speed of sound, allowing their use by the scientific instruments. [1]

However, there is still an issue related to the storage of the hydrogen gas used to produce the proton beam. At first, a gas cylinder containing 5 liters of  $H_2$  with a

pressure level of 150 bar was projected, but the local regulation established that the pressure limit on safe operation (no pressure code requirements AFS2019) is 1.45 bar. Therefore, in this scenario, the solid-state storage through metallic hydrides would be an excellent alternative to enable a higher volumetric density and lower hydrogen pressure than the traditional storage in gaseous form using pressure vessels. A secondary and relevant motivation for the hydrides option is the placement of the gas source inside a high voltage cage (75 kV) were ATEX rules are applied also.

The metallic hydrides are formed by the exothermic, spontaneous, and reversible reaction of the metal with the hydrogen gas, according to Equation 1. [2]



The thermodynamic characteristics of hydride formation are described by pressure-composition-temperature (PCT) diagrams, which show the hydrogen equilibrium pressure as a function of the amount of hydrogen in the metal at a given temperature. When hydrogen gas is applied, the chemical dissociation of the H<sub>2</sub> molecules into hydrogen atoms occurs, which will be adsorbed on the metal surface. Thus, hydrogen atom diffuses into the metal and occupies interstitial sites randomly in the structure, forming a solid solution ( $\alpha$ -phase). [3] The  $\alpha$ -phase is capable of absorbing a maximum quantity of hydrogen, which is proportional to the hydrogen pressure, as given by Sievert's Law [4] (Equation 2):

$$c\left(\frac{H}{M}\right) = K\sqrt{pH_2} \quad (2)$$

Where  $c(H/M)$  is the solubility limit,  $K$  is a constant temperature-dependent, and  $pH_2$  is the hydrogen pressure.

As the hydrogen pressure increases, reaching the solubility limit, the hydride ( $\beta$ -phase) nucleation begins. While the solid solution and the hydride coexist, a pressure plateau appears in the isotherms, which length determines the amount of hydrogen stored. Finally, when the solid solution is entirely converted to hydride, the pressure increases abruptly with the hydrogen concentration. Hence, below the plateau pressure ( $P_{plat}$ ), only the solid solution will be in equilibrium with H<sub>2</sub> gas, and above the plateau, only the hydride will be in equilibrium with H<sub>2</sub> gas.

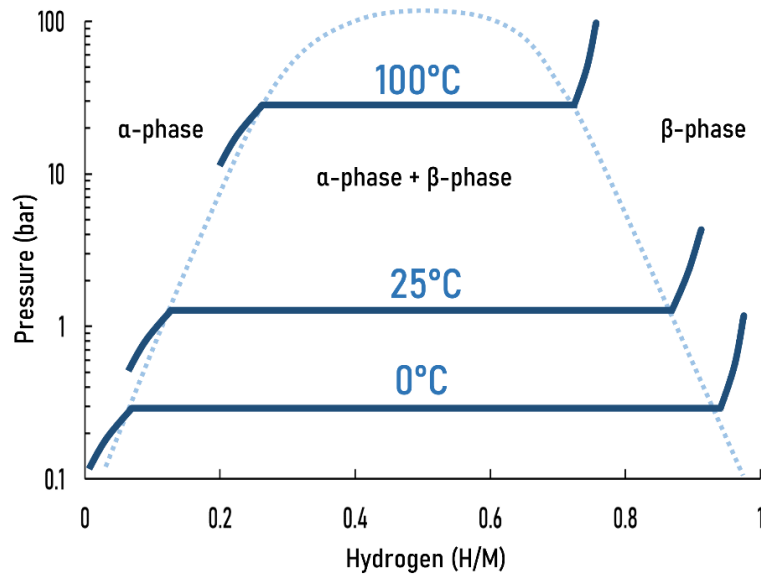


**Figure 2:** Pressure-composition isotherms for a hypothetical metal-hydrogen system.

In many systems, the plateau pressure in absorption is higher than in desorption, as shown in figure 3. This phenomenon is known as hysteresis and is generally explained by the occurrence of irreversible plastic deformation due to the lattice expansion upon hydrogen absorption. Therefore, it is inferred that the true equilibrium is situated somewhere between the absorption and desorption plateaus. [2,5]. It is also commonly possible to see sloppy plateaus, often related to inhomogeneity in the alloy composition. However, this behavior is also seen in pure metals, which is presumed related to constraints caused by the hydrogen insertion and removal in the metal lattice.

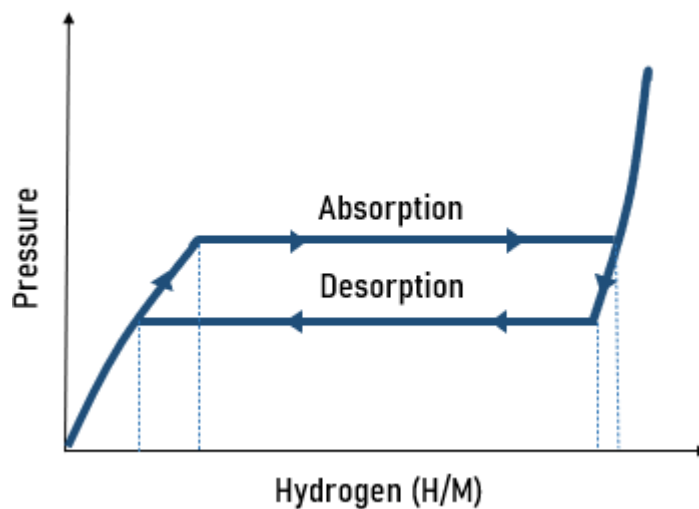


**Figure 3:** Schematic pressure-composition isotherms hysteresis.

## 2. Problem Statement

Regarding the European Spallation Source scenario, this work aims to design a tank to store the equivalent of 5 liters of hydrogen pressurized at 150 bar (corresponding to 0.75 m<sup>3</sup> of hydrogen at room temperature and 1 bar) in solid-state using a metal hydride, ensuring that the pressure level will be maintained below 1.45 bar. For this, some requirements need to be met: the operating temperature at ESS is 15°C, but temperatures up to 25°C need to be considered in case of variations. Besides, the application requires a hydrogen flow of 3.8 x 10<sup>-4</sup> cm<sup>3</sup>/s, and the external pressure is about 5 x 10<sup>-8</sup> bar (operational pressure of the ion source). Finally, a security evaluation needs to be done, predicting the hydride behavior and security in contact with air.

Hence, a metallic alloy will be selected considering the desirable properties and the requirements described, and the tank will be designed and sized. Finally, a cost analysis of the tank's production will be made, including proposals of a prototype and proof of concepts tests to evaluate the designed characteristics.

## 3. Material selection

First, selecting a suitable alloy to store hydrogen in the tank was indispensable regarding the desirable properties and the application conditions. Then, to ensure that the tank pressure will not surpass 1.45 bar at the application temperature (15°C), it is needed a hydride that has a plateau pressure below 1.45 bar at the same temperature, because above the plateau pressure, the metal hydride is formed, and the plateau pressure is maintained. In addition, considering possible temperature deviations, it is sought a hydride with a plateau pressure below 1.45 at 25°C.

However, it is not desirable to have a plateau pressure extremely low because it would be challenging to attain a pressure below the plateau to desorb the hydrogen. In this case, increasing the temperature to elevate the plateau pressure and allow hydrogen desorption would be necessary. However, this temperature increase is not advantageous for the studied application at ESS. So, it is desired to investigate a hydride that absorbs and desorbs hydrogen at 15°C. Moreover, the application requires a hydrogen flow of 3.8 x 10<sup>-4</sup> cm<sup>3</sup>/s, which is directly related to the desorption

kinetics of the alloy. This property needs to be evaluated experimentally, so section 7.4 details an experiment to be done in the future.

There are a wide range of up-and-coming systems in the solid-state hydrogen storage field, like complex hydrides (mainly those based on Mg, Al, and Li), Mg-based hydrides, intermetallic hydrides of the AB, A<sub>2</sub>B, AB<sub>2</sub>, and AB<sub>5</sub> families, such as TiFe, Mg<sub>2</sub>Ni, ZrV<sub>2</sub> and LaNi<sub>5</sub>, and body-centered cubic solid solutions hydrides.[3,5] Besides, a new class of materials, the high entropy alloys (HEAs), have attractive hydrogen storage properties. These alloys are composed of at least three elements with considerable atomic fractions [6].

The balance between non-hydride-forming and hydride-forming alloys is significant for tailoring the hydrogen storage properties of high entropy alloys. Strozi et al. [7] studied the effects of chromium content, a non-hydride-forming element, on the hydrogen storage properties of (TiVNb)<sub>100-x</sub>Cr<sub>x</sub> high entropy alloys. Three different alloys were investigated: (TiVNb)<sub>85</sub>Cr<sub>15</sub>, (TiVNb)<sub>75</sub>Cr<sub>25</sub>, and (TiVNb)<sub>65</sub>Cr<sub>35</sub>. All three alloys were synthesized by arc melting and showed a major body-centered cubic (BCC) phase. Besides, the alloys absorbed hydrogen at room temperature (~24°C) without any activation treatment, presenting a maximum absorption capacity of about H/M = 2 and forming a face-centered cubic (FCC) hydride.

The authors reported that the absorption plateau pressure increased by increasing the Cr/(TiNbV) ratio. The pressure-composition isotherms of the three alloys at 24°C are shown in figure 4. It is possible to see that (TiVNb)<sub>65</sub>Cr<sub>35</sub> alloy has a plateau pressure of absorption very close to 1 bar (100 kPa), and the plateau pressure of desorption is about one order of degree smaller, 0.1 bar (10 kPa), forming a significant hysteresis. Moreover, the reversible capacity, approximately given by the desorption plateau width, is about 1.0 H/M.

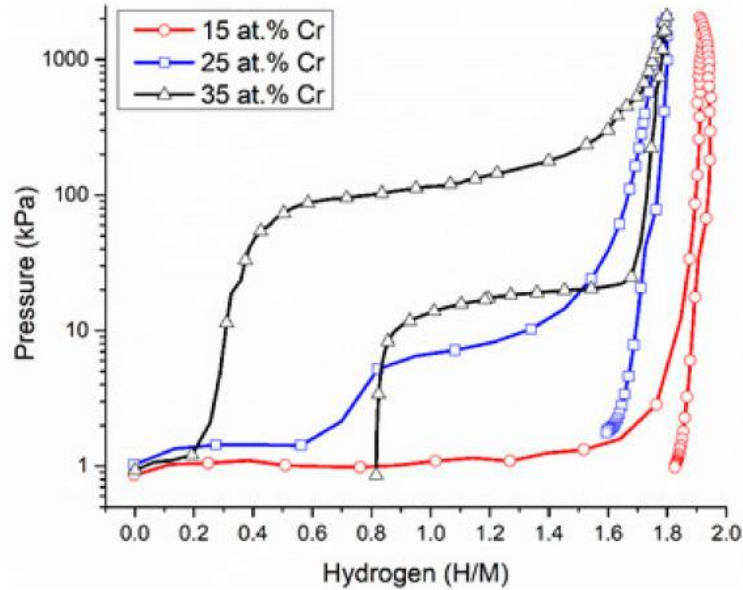


**Figure 4:** PCI absorption/desorption isotherms at 24°C. [7]

Therefore,  $(\text{TiVNb})_{65}\text{Cr}_{35}$  alloy seems to have attractive features for the application in the tank, showing the plateau of absorption close to 1 bar and both absorbing and desorbing hydrogen at room temperature. However, as the normal temperature in ESS is 15°C, it is crucial to know the plateau pressure at this temperature, as well as the reversible capacity of storage. So, the chromium content must be tuned to obtain a plateau pressure of  $(\text{TiVNb})_{100-x}\text{Cr}_x$  alloy at 15°C close to 1 bar, also ensuring that the plateau pressure will not surpass 1.45 bar at 25°C.

For the composition tuning, will be employed a thermodynamic model described by Zepon et al. [8]. The model calculates the PCT diagrams of body-centered multicomponent alloys based on their chemical composition and hydrogen content. This possibility is advantageous since the experimental measurements are very time-consuming, and experimentally investigating many compositions would be unfeasible.

In summary, the model proposes calculating the Gibbs free energy, assuming that the hydrogen partial molar enthalpy is constant for a given phase. Consequently, the enthalpy of hydrogen mixing varies linearly with the hydrogen content. Besides, considering a multicomponent alloy, the hydrogen partial enthalpy of a phase was approximated by a simple ideal mixture law of this quantity for the alloy's components with the same structure. Finally, the entropy of the phases was described based on the ideal configurational entropy for interstitial solid solutions with site blocking effect, which considers that the occupation of an interstitial site is blocked by the previous occupation of a neighboring site.

The thermodynamic model showed a remarkable agreement with the experimental results for the TiVNbCr system. In addition, the authors reported that the calculated plateau is between the absorption and desorption plateaus for the  $(\text{TiVNb})_{85}\text{Cr}_{15}$  alloy, as shown in figure 5, which is associated with the hypothesis that the true equilibrium occurs between both plateaus.

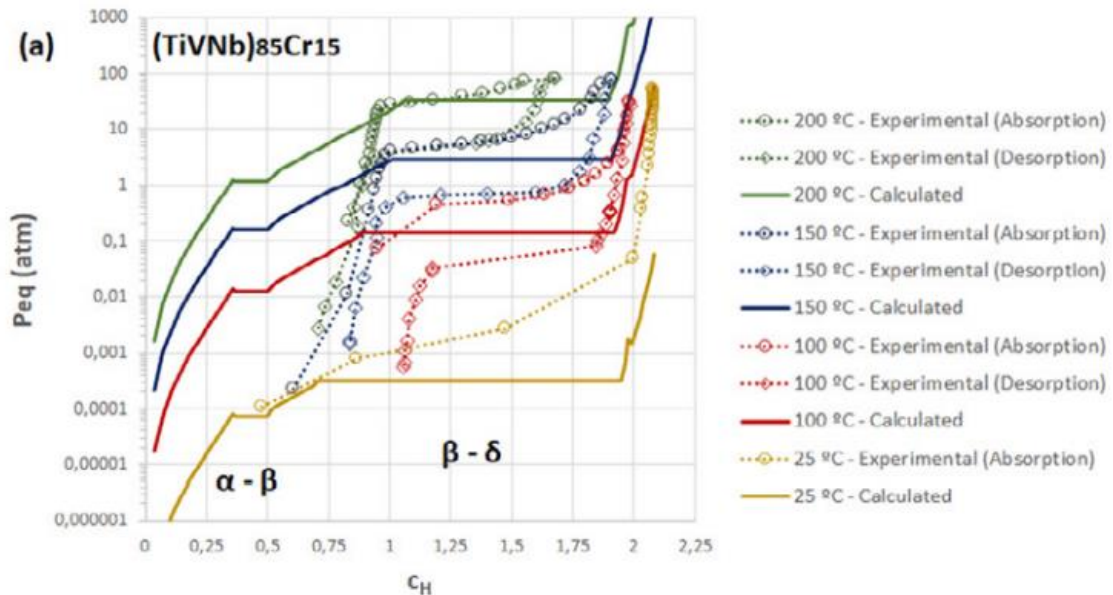


**Figure 5:** Comparison between experimental and calculated PCI diagrams of  $(\text{TiVNb})_{85}\text{Cr}_{15}$  [8]

Besides, the agreement is also excellent for the  $(\text{TiVNb})_{65}\text{Cr}_{35}$  alloy. The PCI diagram shown in figure 6 was calculated based on the exact chemical composition of the  $(\text{TiVNb})_{65}\text{Cr}_{35}$  alloy measured by Energy Dispersive Spectroscopy in Strozi et al. work [7], enabling a reliable comparison with the experimental PCT diagram exhibited in figure 3. The calculated plateau pressure (1.02 bar) is close to the experimental plateau pressure in absorption ( $\sim 1$  bar).



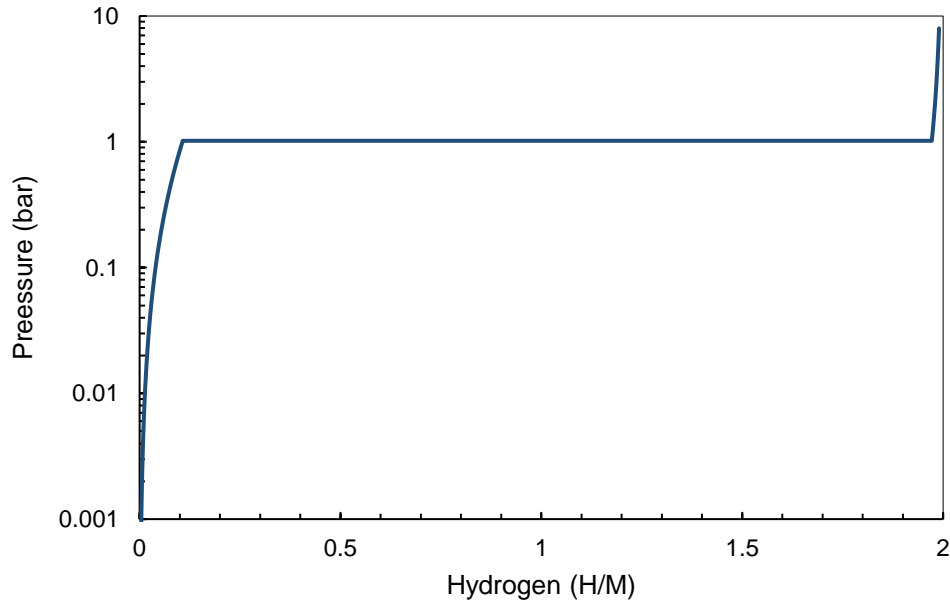


**Figure 6:** PCI diagram calculated for the  $(\text{TiVNb})_{65}\text{Cr}_{35}$  alloy.

Based on these notable results, it is clear that the referred thermodynamic model is a great tool to predict the plateau pressure of different chromium contents in  $(\text{TiVNb})_{100-x}\text{Cr}_x$  alloy. As the calculated plateau pressures are in between the absorption and desorption plateaus, for sure, the desorption plateau will always be below the calculated plateau pressure. It is also important to highlight that the  $(\text{TiVNb})_{100-x}\text{Cr}_x$  alloy shows a large hysteresis, with approximately one degree of difference between the absorption and the desorption plateaus, as seen in figure 3. Therefore, if the calculated plateau pressure is below or slightly above 1.45 bar, the alloy can be considered a potential candidate for this project.

First, the PCI diagrams were calculated at  $15^\circ\text{C}$  for five different values of chromium atomic percentage: 35%, 34.5%, 34%, 33.5%, and 33%. The results are exhibited in figure 7.

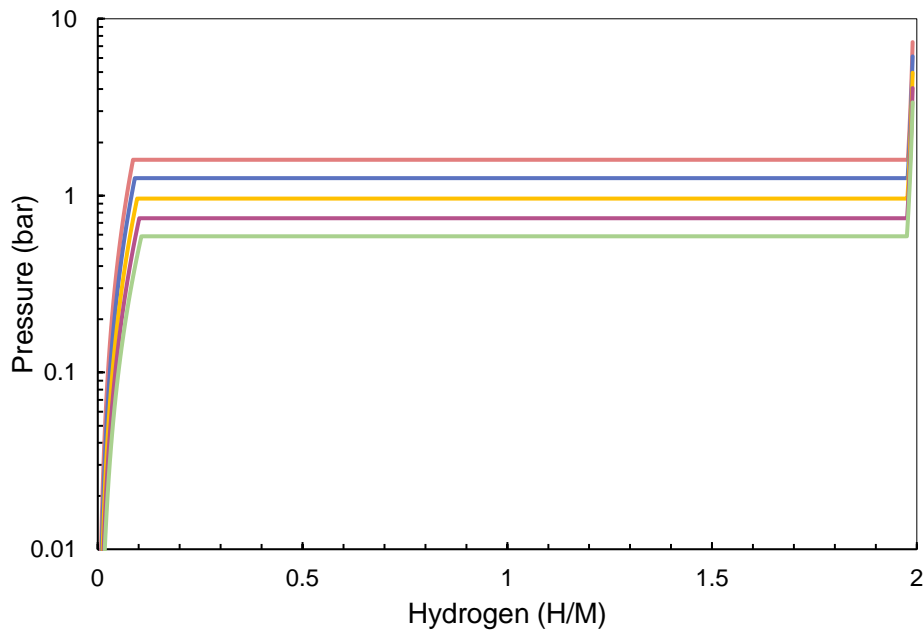


**Figure 7:** PCI diagram calculated for five different compositions at 15°C

It is possible to eliminate the  $(\text{TiVNb})_{65}\text{Cr}_{35}$  alloy from the list of candidates since the plateau pressure reaches 1.61 bar, i.e., it is higher than the maximum pressure demanded (1.45 bar). Then, the PCI diagrams at 25°C were calculated, which results are demonstrated in figure 8.

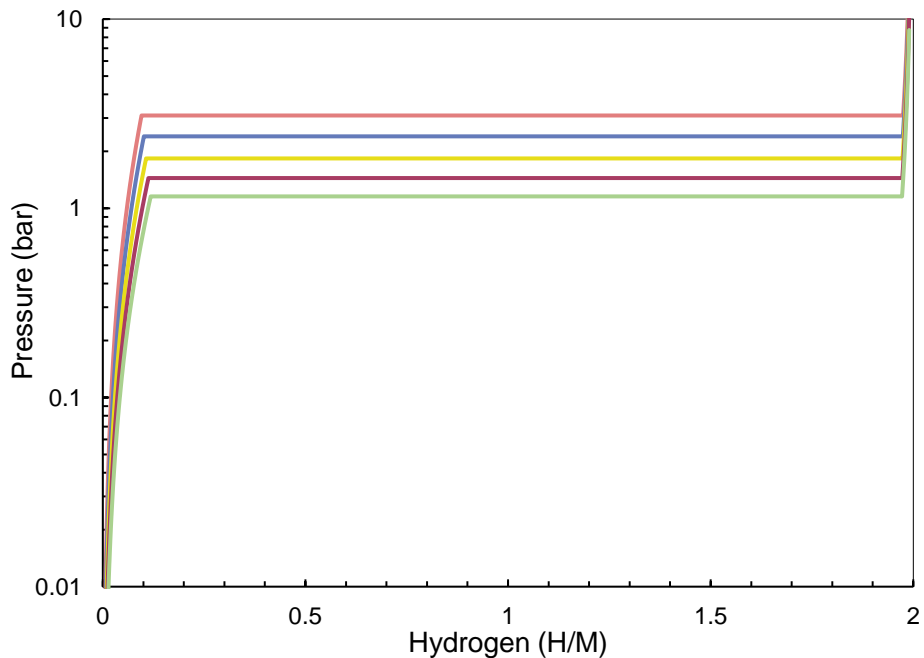


**Figure 8:** PCI diagram calculated for five different compositions at 25°C

In this second analysis,  $(\text{TiVNb})_{65}\text{Cr}_{34.5}$ ,  $(\text{TiVNb})_{66}\text{Cr}_{34}$ , and  $(\text{TiVNb})_{66.5}\text{Cr}_{33.5}$  alloys can be excluded from the candidate's list, with plateau pressures equals to 2.43

bar, 1.88 bar, and 1.47 bar, respectively. Therefore, it is possible to conclude that the  $(\text{TiVNb})_{67}\text{Cr}_{33}$  alloy is a suitable choice for this project since the calculated plateau pressure is equal to 1.17 bar at 25°C, ensuring that the pressure will not surpass the maximum pressure at this temperature. All the plateau pressures obtained for each alloy at 15°C and 25°C are presented in table 1.

**Table 1:** Plateau pressures at 15°C and 25°C for all the analyzed compositions.

<b>Alloy</b>	<b>P<sub>plat</sub> at 15°C (bar)</b>	<b>P<sub>plat</sub> at 25°C (bar)</b>
<b><math>(\text{TiVNb})_{65}\text{Cr}_{35}</math></b>	1.61	3.05
<b><math>(\text{TiVNb})_{65.5}\text{Cr}_{34.5}</math></b>	1.28	2.43
<b><math>(\text{TiVNb})_{66}\text{Cr}_{34}</math></b>	0.97	1.88
<b><math>(\text{TiVNb})_{66.5}\text{Cr}_{33.5}</math></b>	0.76	1.47
<b><math>(\text{TiVNb})_{67}\text{Cr}_{33}</math></b>	0.60	1.17

#### 4. Tank sizing

Once the alloy was selected, it was possible to determine the mass and volume needed. Nevertheless, first, it was necessary to know the mass of hydrogen that will be stored, based on the parameters informed by the ESS team. A 5l cylinder at 15°C and pressurized at 150 bar is being considered. Considering that the volumetric density of hydrogen in these conditions is 11.54 kg/m<sup>3</sup> [9], the hydrogen mass in the cylinder currently in use is 57.70 g. As a result, the alloy mass and volume needed to store this quantity of hydrogen could be found.

##### 4.1 Alloy's mass calculation

In general, the reversible hydrogen storage capacity is less than the maximum capacity and is estimated as the plateau width in the PCT curve. This is related to the different stages of the hydrogenation reaction. In BCC alloys, a solid solution ( $\alpha$ -phase) is formed first, then a monohydride ( $\beta$ -phase), and, finally, a dihydride ( $\gamma$ -phase). It is known that the equilibrium pressure of transformation from  $\alpha$ -phase to  $\beta$ -phase is very low at room temperature due to its high stability. Thus, the high-temperature application is required for hydrogen desorption from the  $\beta$ -phase to occur, so only the hydrogen absorbed in the transformation from monohydride to dihydride is desorbed at sufficiently low temperature and desired pressure. [10–12]

Therefore, using the PCI curve obtained by the thermodynamic model for the  $(\text{TiVNb})_{67}\text{Cr}_{33}$  alloy, presented in figure 9, the alloy's estimated reversible capacity is 3.02%wt at 15°C.

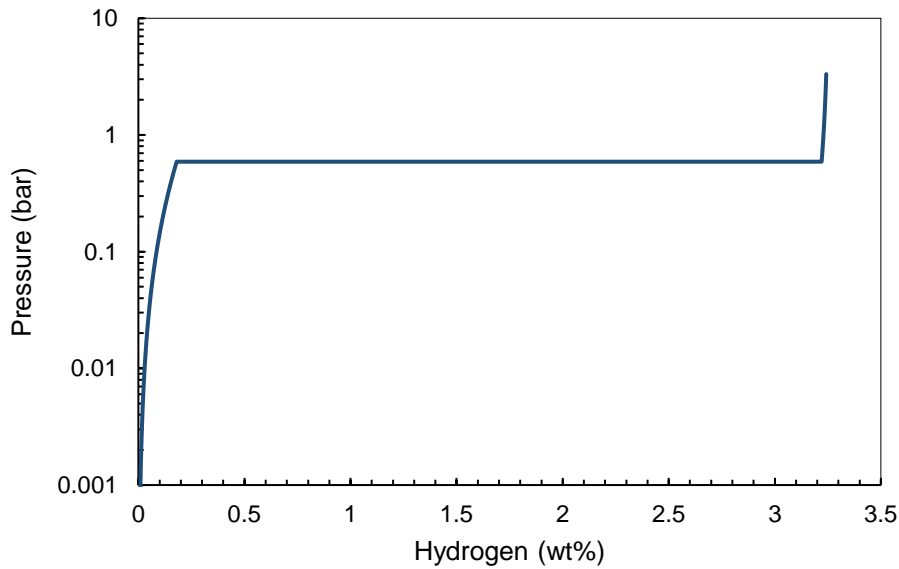


**Figure 9:** PCT diagram of  $(\text{TiVNb})_{67}\text{Cr}_{33}$  at 15°C obtained by the thermodynamic model.

So, the hydride mass needed to store 57.70g of hydrogen can be calculated using the reversible capacity through Equation 3, resulting in 1.911 kg.

$$\%wt = \frac{\text{hydrogen mass(g)}}{\text{hydride mass(g)}} \times 100\% \quad (3)$$

#### 4.2 Alloy's volume calculation

The hydride volume was calculated using the theoretical density of  $(\text{TiVNb})_{67}\text{Cr}_{33}$  hydride, given by Equation 4:

$$\rho = \frac{n_M A_M + n_H A_H}{V_c N_A} \quad (4)$$

where  $n_M$  and  $n_H$  are the numbers of metal atoms and hydrogen atoms associated with each unit cell, respectively,  $A_M$  and  $A_H$  are the atomic weight of the alloy atoms and the hydrogen atom, respectively,  $V_c$  is the volume of the unit cell, and  $N_A$  is the Avogadro's number ( $6.022 \cdot 10^{23}$  atoms/mol).

The unit cell volume was determined using the estimated lattice parameter of the  $(\text{TiVNb})_{67}\text{Cr}_{33}\text{H}_x$  hydride. Strozi et al. [7] showed that the lattice parameter of  $(\text{TiVNb})_{100-x}\text{Cr}_x$  decreases with the Cr content because of the smaller atomic radius of Cr compared to the other elements in the alloy. Because of that, the lattice parameter decreases from 3.158 Å for BCC  $(\text{TiVNb})_{85}\text{Cr}_{15}$  alloy to 3.105 Å for BCC  $(\text{TiVNb})_{65}\text{Cr}_{35}$  alloy. Besides, Silva et al. [6] obtained  $a = 4.405$  Å for the  $(\text{TiVNb})_{85}\text{Cr}_{15}\text{H}_x$  hydride. So, it may be inferred that a lattice parameter value of 4.357 Å is a suitable approximation to the lattice parameter of  $(\text{TiVNb})_{67}\text{Cr}_{33}\text{H}_x$  hydride, corresponding to a unit cell volume of 82.711 Å<sup>3</sup>.

The hydrogen atoms occupy all the eight tetrahedral interstitial sites in the FCC unit cell [13]. Thus, each FCC unit cell has four metal atoms and eight hydrogen atoms. The atomic weight of the alloy atoms was obtained from the weighted mean of the atomic weights of each element in the alloy, resulting in  $A_M = 59.98$  g/mol, while the atomic weight of hydrogen is  $A_H = 1.008$  g/mol.

Performing the calculation based on equation 2 and the parameters already pointed out, the theoretical density of  $(\text{TiVNb})_{67}\text{Cr}_{33}\text{H}_x$  hydride obtained was equal to 4.98 g/cm<sup>3</sup>. Therefore, once the alloy mass calculated previously is 1.911 kg, the calculated alloy volume is 384 cm<sup>3</sup>.

The experimental results for the  $(\text{TiVNb})_{65}\text{Cr}_{35}$  alloy obtained by Strozi et al. [7] showed a reversible capacity of half the maximum capacity ( $H/M \sim 1$ ). However, the estimated reversible capacity for the  $(\text{TiVNb})_{67}\text{Cr}_{33}$  alloy was 3.02wt% ( $H/M \sim 1.9$ ). Thus, a factor of safety of 50% was considered having in mind the lower reversibility seen experimentally, resulting in 3.822 kg of  $(\text{TiVNb})_{67}\text{Cr}_{33}\text{H}_x$  hydride, which corresponds to a volume of 768 cm<sup>3</sup>.

In addition, considering that the maximum hydrogen storage capacity of the  $(\text{TiVNb})_{67}\text{Cr}_{33}$  alloy is 3.20 wt.% of hydrogen, as seen in figure 9, the alloy's mass required to fill the sample cylinders is 3.70 kg.

## 5. Tank project

A tank was designed to store 768 cm<sup>3</sup> of the  $(\text{TiVNb})_{67}\text{Cr}_{33}\text{H}_x$  hydride based on Swagelok fluid systems components. For this, two options were projected, each one having both advantages and disadvantages. Project A is composed of two sample cylinders of 500 cm<sup>3</sup> each. This configuration has the advantage of providing a lower

cost once the number of components required is significantly small. However, as the hydrogenation reaction is strongly exothermic, the sample cylinder heating will be very significant due to its large volume. Consequently, the plateau pressure will rise along with the temperature, and the hydrogen absorption will be interrupted since the system pressure will be lower than the plateau pressure. In this case, it will be necessary to wait until both temperature and plateau pressure slow down, and then the absorption restarts. Some refrigeration accessories can bypass this problem, like a water coil around the sample cylinders during the hydrogenation process. It is essential to point out that this problem would affect only the production and filling process of the tank but not its operation in the ESS facility. The 3D drawing of project A is shown in figure 10.



**Figure 10:** 3D drawing of project A, with two sample cylinders of 500cm<sup>3</sup>.

On the other hand, project B comprises five sample cylinders of 150 cm<sup>3</sup>, totaling 750 cm<sup>3</sup>. The main advantage of this project is that the hydrogenation in segmented volumes of 150 cm<sup>3</sup> will provide more accurate control of the process once

the cylinder heating is considerably lower than in project A. However, the cost of project B will be higher since it requires a more significant number of components to be constructed. The 3D drawing of project B is shown in figure 11.

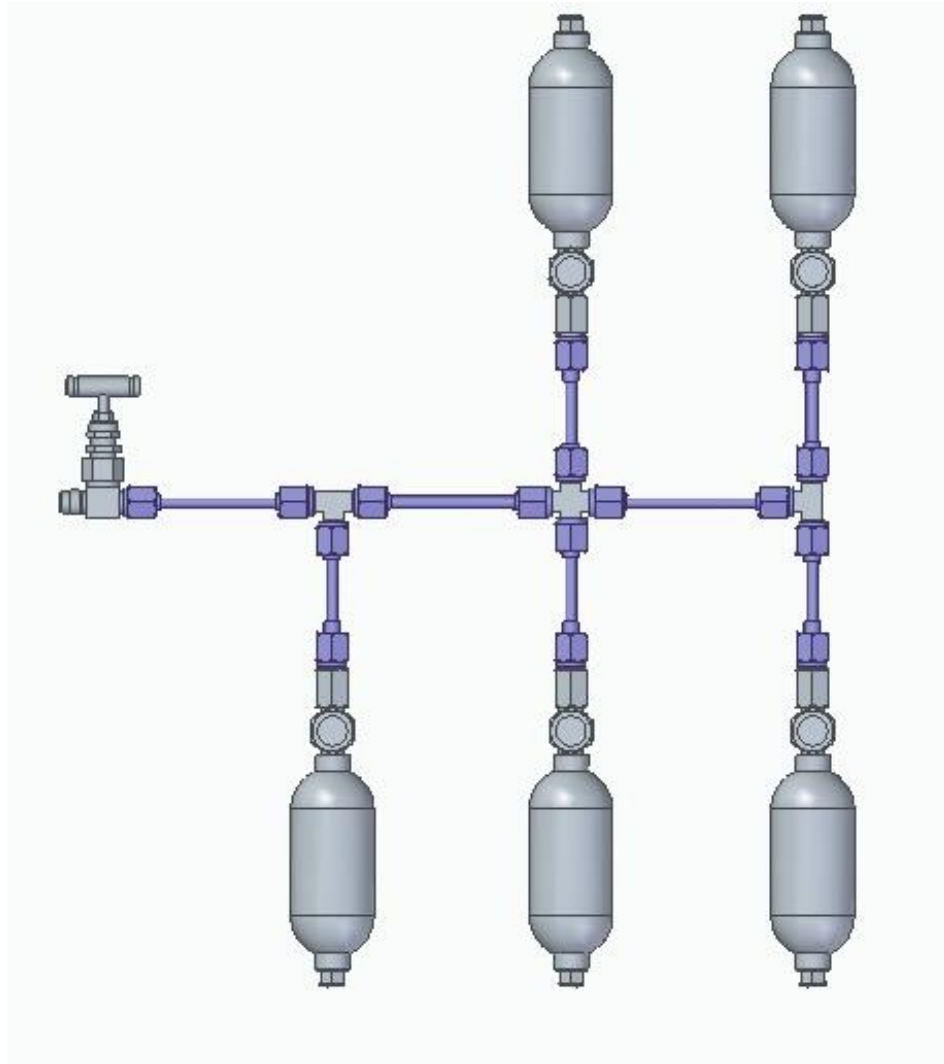


**Figure 11:** 3D drawing of project B, with five sample cylinders of 150cm<sup>3</sup>.

## 5.1 Components detailing

### a) Sample Cylinders

Two sample cylinders with different volumes were selected, one for each project. Their specifications are presented in figure 12. Both cylinders are TPED

(Transportable Pressure Equipment Directive) compliant for secure samples in Europe.

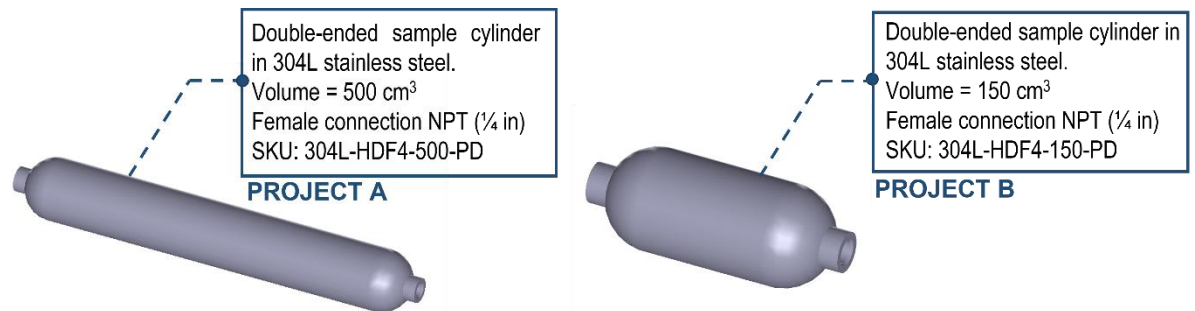


**Figure 12:** Sample cylinders specifications.

Once the cylinders are double-ended, a plug is required to close one of the connections as just one is necessary for both projects. The plug specifications are demonstrated in figure 13.

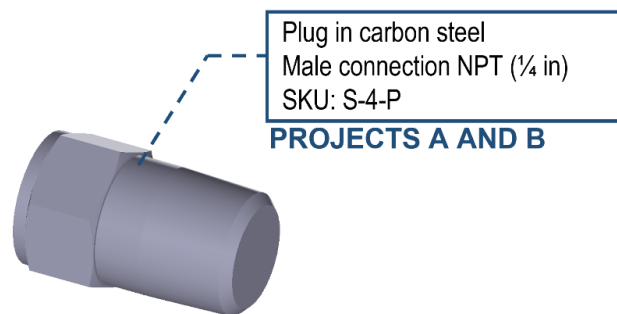


**Figure 13:** Plug in carbon steel specifications.

## **b) Connections**

For both projects, the VCR metal gasket face seal fittings were chosen due to the leak-tight service in vacuum and high pressures, as well as the high purity provided by the metal-to-metal seal. The VCR connection is typically composed of a female nut, a gland, a gasket, and a body. However, it is also possible to use a gland and a male nut instead of a body.

The components chosen for both projects are presented in figures 14 and 15. Three types of bodies were selected as a function of the type of union they can provide for each project. The selected gland is suitable for tube socket weld in one of the connections. This type of welding was selected because it provides excellent tightness, an essential feature for a hydrogen system.



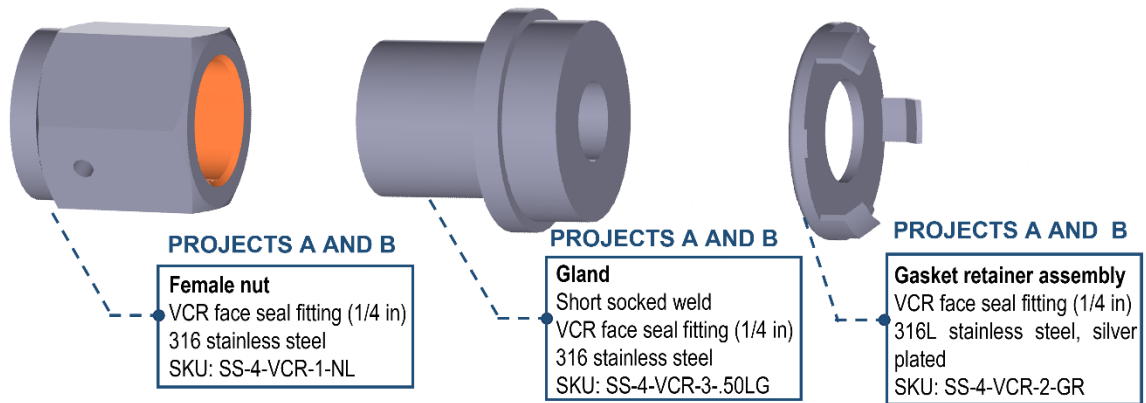


**Figure 14:** VCR components specifications – female nut, gland, and gasket.

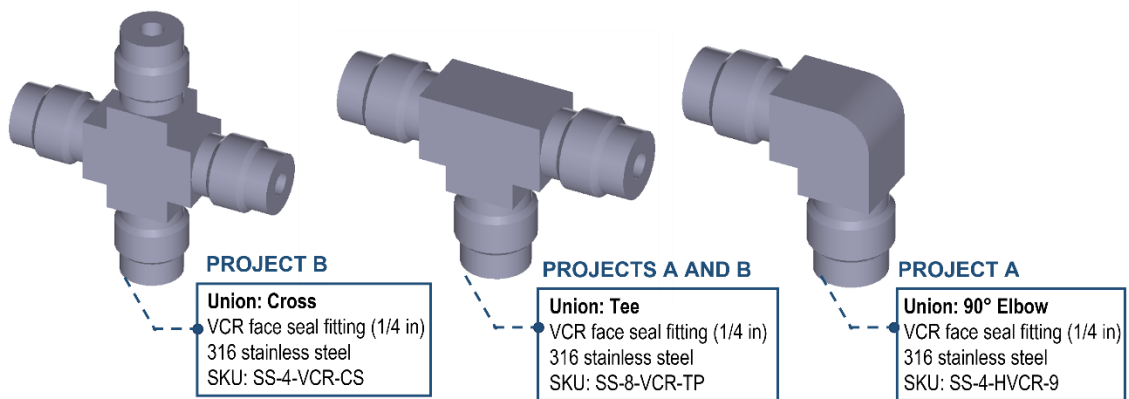


**Figure 15:** VCR bodies specifications – cross, tee, and elbow.

### c) Valves

Valves were needed in two different locations for both projects: at the end of the system and separating each sample cylinder. The valve chosen to control the hydrogen flow to the outside of the system was a needle valve, which provides a reliable and accurate flow control with a smooth and gradual adjustment. This is essential to allow the obtention of the required flow rate in the application. Besides, the needle valve chosen has a maximum working temperature of 232°C and a maximum pressure of 284 bar (no minimum pressure was specified).

The valve selected to separate the sample cylinders was a ball valve. This type of valve is projected to work in the positions opened or closed, the exact function needed in this point of the system: the sample cylinders will be transported with the valves closed and, after their installation in the system, all the ball valves will be opened and left in this position. In addition, this type of valve has the advantage of

high control against leakage in both positions and has a working pressure up to 206 bar (no minimum pressure was specified).

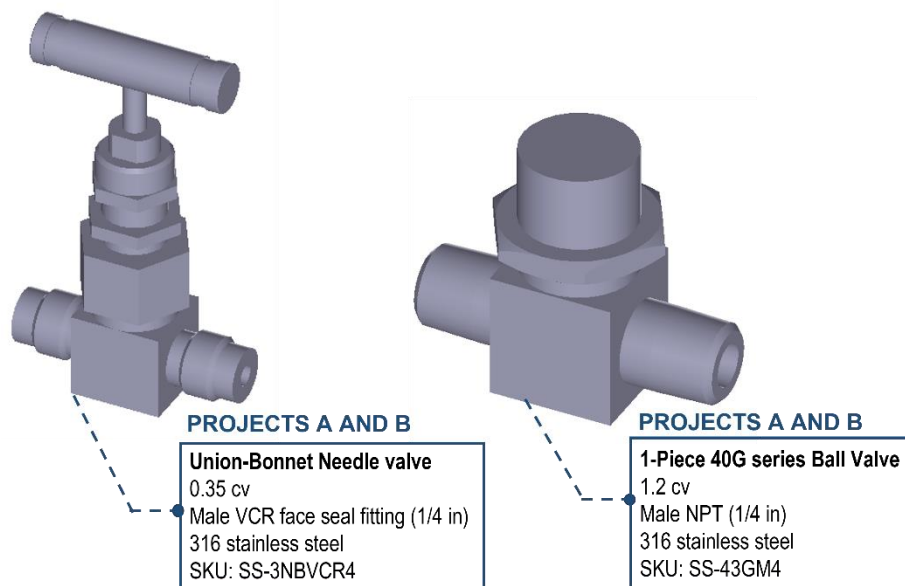


**Figure 16:** Valves specifications – needle valve and ball valve

Once the ball valve has a male NPT connection to provide the fitting with the sample cylinder (female NPT), a body with both female NPT and VCR connections was selected to link the ball valve and the tube with a VCR fitting, as shown in figure 17.

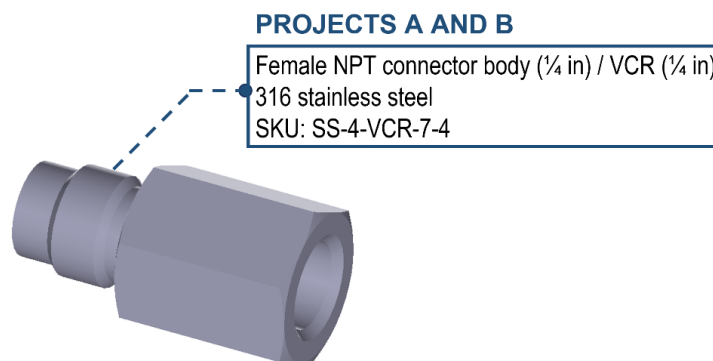


**Figure 17:** Female connector (NPT/VCR) body specification.

#### d) Tubing

For both projects, it was selected a seamless tubing in 316 stainless steel. The tube wall choice was based on the Swagelok recommendations: for gas services, such as hydrogen and helium, as the tube diameter (OD) increases, the probability of a surface defect harms the sealing also increases, since hydrogen gas has tiny molecules that escape in minimal defects. Therefore, an adequate tube wall thickness needs to be selected for each tube diameter, according to a table presented in the Swagelok tubing catalog [14]. For an OD equal to  $\frac{1}{4}$  in, a tube wall of 0.028 in was chosen, allowing working pressures up to 276 bar. Besides, for both projects, the necessary tubing length is 1 meter, the minimum length available for purchase.

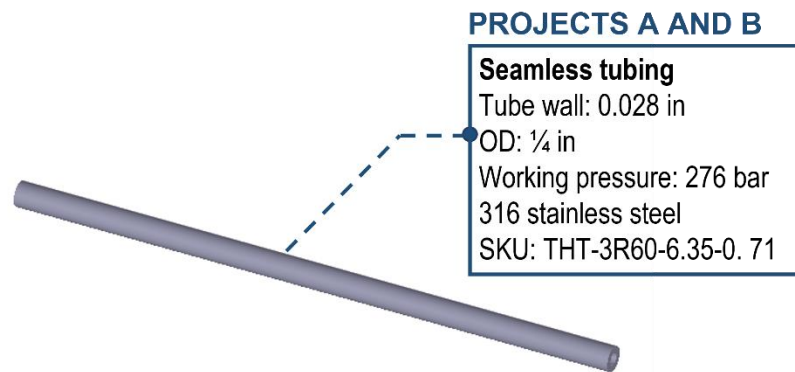


**Figure 18:** Seamless tubing specifications.

### 5.2 Procedure after the hydrogen depletion

To define the procedure adopted after the hydrogen depletion, i.e., when the tank must be replaced after delivering all available  $H_2$ , it is crucial to analyze the  $(TiVNb)_{67}Cr_{33}H_x$  cyclability, i.e., the capacity to absorb/desorb hydrogen multiple times with no significant loss of storage capacity.

Several studies seek to understand the causes of the significant loss of hydrogen storage capacity over the number of absorption/desorption cycles in BCC alloys. Young et al. [15] pointed out as one of the causes of cyclic degradation the fact that the structure does not entirely return to BCC or BCT after hydrogen desorption,

existing a combination of BCC or BCT and FCC structures, due to the greater stability of this structure compared to the other two. Furthermore, Selvaraj et al. [16] reported that the loss of capacity in the Ti-V-Cr system occurs due to disproportionation of the alloy composition, leading to a precipitation of vanadium and titanium in each cycle which form their respective hydrides. The high stability of such hydrides causes the drop in storage capacity in each cycle, desorbing hydrogen only at temperatures above 400°C, outside the range studied. Other authors have also reported this effect [17–19] as a hypothesis for cyclic degradation. Finally, several authors have reported a relationship between the hydrogenation reaction in steps and the low reversibility of BCC alloys, which results only in the desorption of the hydrogen absorbed in the transformation from monohydride to dihydride, leading to a lower capacity in the following cycles.[10–12]

Silva et al. [6] measured the hydrogen absorption/desorption cycling for the  $(\text{TiVNb})_{85}\text{Cr}_{15}$  alloy. The authors reported that the alloy continuously reduced storage capacity from 3.18wt% to 2.88wt% after 20 cycles, as shown in figure 19. Thus, it is possible to see that the  $(\text{TiVNb})_{85}\text{Cr}_{15}$  alloy has the best cyclability in the study.

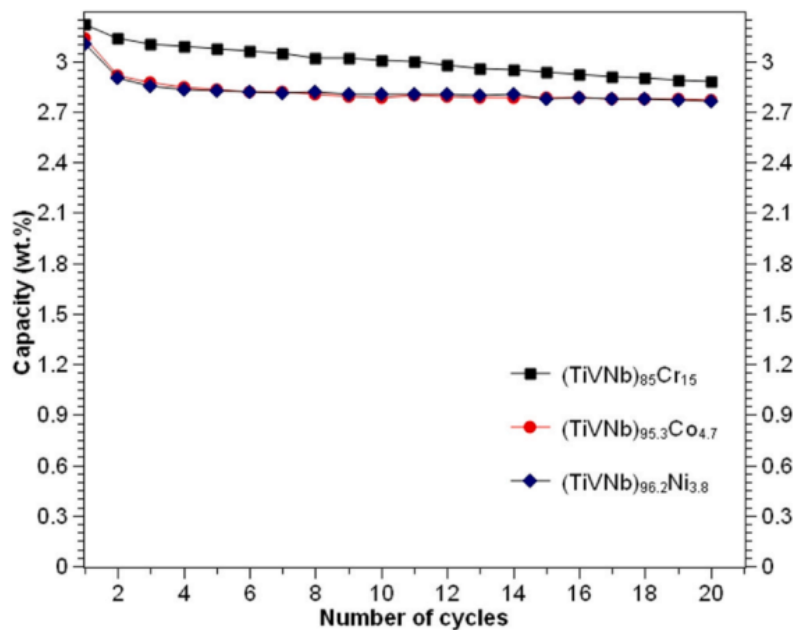


**Figure 19:** Hydrogen absorption capacity in wt% of  $(\text{TiVNb})_{85}\text{Cr}_{15}$ ,  $(\text{TiVNb})_{95.3}\text{Co}_{4.7}$ , and  $(\text{TiVNb})_{96.2}\text{Ni}_{3.8}$  alloys as a function of cycles of absorption and desorption.[6]

Considering that a factor of safety of 50% was taken into account for the tank sizing in this work, if the cyclability of the  $(\text{TiVNb})_{67}\text{Cr}_{33}$  alloy is similar to the  $(\text{TiVNb})_{85}\text{Cr}_{15}$  alloy or even slightly lower, it is possible to ensure that the hydride can be subjected to several cycles of absorption and desorption maintaining the ideal

quantity of hydrogen stored. Initial results obtained at the Laboratory of Hydrogen in Metals (LH<sub>2</sub>M) of DEMa-UFSCar have shown that the (TiVNb)<sub>65</sub>Cr<sub>35</sub> alloy has excellent cyclability at room temperature, with no loss of the reversible capacity after several cycles of absorption and desorption. However, measuring the (TiVNb)<sub>67</sub>Cr<sub>33</sub> cyclability is still necessary to precisely predict the maximum number of cycles that provide the required storage capacity.

## 6. Cost projection

The cost analysis for the tank production involved the costs for the alloy synthesis and the tank construction considering each Swagelok component.

### 6.1 (TiVNb)<sub>67</sub>Cr<sub>33</sub> synthesis

The prices of the pure elements Ti, Nb, V, and Cr were obtained on the Alfa Aesar website, which is a significant supplier of pure metals, research chemicals, and materials. The chosen metals specifications are presented in table 2.

**Table 2:** Pure metals specifications – titanium, niobium, vanadium, and chromium

Metal	Type	Trace metals
Titanium	Granules	99.9%
Niobium	Pieces	99.8%
Vanadium	Pieces	99.7%
Chromium	Pieces	99%

The prices per gram of each element were obtained, and the total price was calculated based on the required mass of each one. It is important to emphasize that the masses are adjusted according to the quantities available on the website.

**Table 3:** Required mass, price per gram, and the total price of each pure element.

	Mass (g)*	Price per gram (US\$/ g)	Total price (US\$)
Titanium	850	1.09	928.00
Niobium	900	0.949	854.00
Vanadium	850	2.880	2,448.00
Chromium	1,300	0.365	474.00
<b>(TiVNb)<sub>67</sub>Cr<sub>33</sub></b>			<b>4,704.00</b>

\*The masses were determined based on the available packages for acquisition on the Alfa Aesar website.

Considering a US Dollar to Brazilian Real exchange rate equal to 5.51 on 10/10/2021, the total price in Brazilian Real is R\$ 25,919.04. Besides, an importation tax needs to be considered for the (TiVNb)<sub>67</sub>Cr<sub>33</sub> synthesis in Brazil, 60% of the product value plus shipping charges. However, the tax value cannot surpass R\$3,000.00, so, in this case, the tax will be equal to R\$3,000.00, resulting in R\$28,919.04, not counting shipping charges and the ICSM tax.

Moreover, there is also the cost of the alloy's synthesis by electric arc melting in vacuum. This process provides high chemical homogeneity, oxide cleanliness, and reduction of impurities. However, the cost depends on where the synthesis will be carried out, and this decision will be made in the future.

## 6.2 Tank components

The components' unit prices and their required quantity for each project are shown in table 4, along with the components' total costs of projects A and B.

**Table 4:** Unit prices and the required quantities of each tank component.

Component	SKU	Unit price (R\$)	Project A Quantity	Project B Quantity
Sample Cylinder: 150 cm <sup>3</sup>	304L-HDF4-150-PD	2,531.00	-	5
Sample Cylinder: 500 cm <sup>3</sup>	304L-HDF4-500-PD	2,920.50	2	-
Union: Tee (VCR)	SS-8-VCR-TP	1,664.25	1	3
Union: Cross (VCR)	SS-4-VCR-CS	833.96	-	1
Union: 90° Elbow (VCR)	SS-4-HVCR-9	777.39	1	-
Female nut (VCR)	SS-4-VCR-1-NL	166.65	8	16
Gasket retainer assembly (VCR)	SS-4-VCR-2-GR	69.59	8	16
Gland (VCR)	SS-4-VCR-3-.50LG	253.47	8	16
Union-Bonnet Needle valve	SS-3NBVCR4	3,648.75	1	1
1-Piece 40G series Ball Valve	SS-43GM4	1,362.19	2	5
Seamless tubing Length:1 m	THT-3R60-6.35-0.71	57.84	1	1
Plug (for the sample cylinder)	S-4-P	84.87	2	5
Female conector body NPT / VCR	SS-4-VCR-7-4	296.94	2	5
<b>Total cost (R\$): Project A</b>		<b>R\$19,394.91</b>		

<b>Total cost (R\$): Project B</b>	R\$38,743.66
------------------------------------	--------------

Therefore, projects A and B's components' total costs are R\$19,394.91 and R\$38,743.66, respectively, not counting shipping charges and the ICMS tax. Project B is most expensive than project A due to the most significant number of components required, so it is essential to analyze the pros and cons of each one to make a decision.

## **7. Proposal of a prototype and proof-of-concept tests**

A prototype is an early model of a product created to perform proof-of-concept tests. This project stage is essential to identify possible failures in the initial project and verify experimentally the concepts involved in the product. Hence, a prototype will be proposed in this section. In addition, some proof-of-concept tests will be relevant to enhancing the project since some critical properties only can be known by experimental measurements.

### **7.1 Prototype description**

The prototype will be constructed using a Sievert's Apparatus (Setaram® model PCTPro) available at the Laboratory of Hydrogen in Metals (LH<sub>2</sub>M) of DEMa-UFSCar. This instrument contains two reservoirs of known volume: a sample volume, where the sample is loaded, and a reference volume. Both reservoirs are isolated by a valve, as shown in figure 20. The reference volume is filled with H<sub>2</sub> gas for the hydrogen uptake measurements until the desired pressure is reached. When the isolation valve is opened, a new equilibrium can be established, and the hydrogen sorption by the sample in its volume can be obtained by measuring the pressure variation in the reference volume.

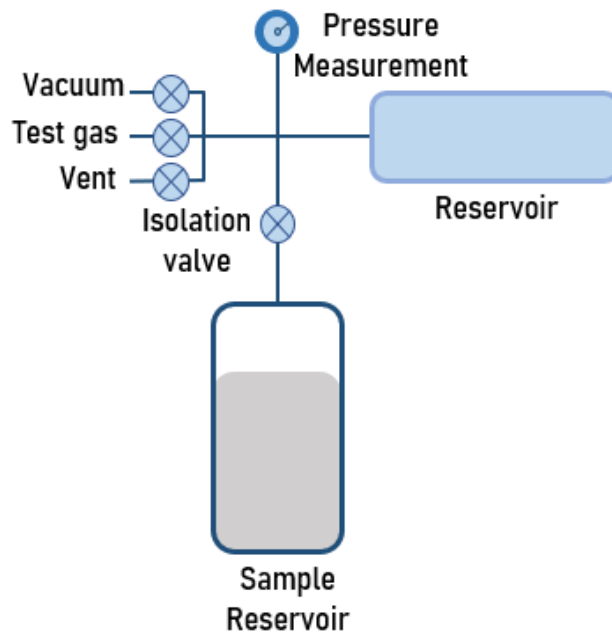


**Figure 20:** Sievert's apparatus scheme.

The sample reservoir will be replaced by a 150 cm<sup>3</sup> sample cylinder as in project B, which will be considered the prototype for proof-of-concept and additional testing. Thus, the (TiVNb)<sub>67</sub>Cr<sub>33</sub> mass needed for the prototype construction is 740g.

## 7.2 Alloy's synthesis and chemical composition verification

The (TiVNb)<sub>67</sub>Cr<sub>33</sub> alloy will be synthesized by electric arc melting under argon atmosphere in an electric arc melting furnace located in the Materials Engineering Department at UFSCar. The ingot will be remelted eight times to ensure chemical homogenization. Subsequently, the sample will be stored in a Mbraun glovebox under argon atmosphere with levels of O<sub>2</sub> and H<sub>2</sub>O lower than 0.5 ppm.

To access the chemical composition and the present phases in the alloy, X-Ray Diffraction (XRD), Scanning Electron Microscopy (SEM), and Energy Dispersive Spectroscopy (EDS) analysis will be performed. For this, the sample will be subjected to a metallographic preparation (sectioning, mounting, grinding, and mechanical polishing).

## 7.3 PCI diagram measurement

Although the PCI diagram for the (TiVNb)<sub>67</sub>Cr<sub>33</sub> was already calculated and predicted for different temperatures, it is crucial to obtain the measured diagram since



the thermodynamic model has some inherent errors that need to be assessed. As a result, the plateau pressures of absorption and desorption can be confirmed, and the reversible capacity of hydrogen storage can be evaluated.

The PCI diagrams will be carried out in a Sievert's apparatus described in section 7.1. The hydrogen absorption is usually not spontaneous due to an oxide layer on the metal surface that significantly hinders hydrogen dissolution in the alloy structure. Therefore, the sample will be subjected to a heat treatment at 400 °C for two hours under a dynamic vacuum, destabilizing the oxide layer and facilitating hydrogen absorption. Only a few milligrams of the alloy are needed for PCI measurements.

The diagrams are obtained with the addition of small doses of H<sub>2</sub> in the reference volume, and after each dose, there is a waiting time until the equilibrium pressure between the sample and the gas is reached. Therefore, the concentration of absorbed H<sub>2</sub> is calculated. The PCI diagram is, essentially, a plot of the absorbed H<sub>2</sub> concentration (H/M or %wt) as a function of the final equilibrium pressure after each dose. For hydrogen desorption, gas is removed from the reference volume in steps, and the equilibrium pressure is measured after the equilibrium pressure between the sample and the gas is achieved.

#### **7.4 Evaluation of the H<sub>2</sub> flow**

Once the application in ESS requires an H<sub>2</sub> flow of  $3.8 \times 10^{-4} \text{ cm}^3/\text{s}$ , it is essential to evaluate the flow in the hydrogen release of the (TiVNb)<sub>67</sub>Cr<sub>33</sub>H<sub>x</sub> hydride. For this, the following procedure will be implemented:

- After PCI measurement, the 150 cm<sup>3</sup> sample cylinder filled with 740g of the alloy will be entirely absorbed by incremental H<sub>2</sub> doses until the alloy is completely absorbed and the cylinder pressure reaches 1 bar. The temperature variation of the cylinder during absorption will be monitored during the absorption procedure.
- Then, the isolation valve that separates the sample and reference reservoirs will be closed, and the reference reservoir will be evacuated.
- After the evacuation, the isolation valve will be open, allowing the start of the hydrogen desorption since the pressure will be lower than the hydride plateau pressure.

- The increase in the reference reservoir pressure will be registered as a function of time. As a result, the hydrogen flow will be assessed.
- In addition, a gas flowmeter can be installed between the sample holder and the reservoir, so the desorption flow rate of the full prototype can be directly measured.

### **7.5 Hydride safety in air contact**

The security in case of hydride contact with air needs to be investigated since accidental valve openings, for example, are possible. Therefore, it is essential to predict the hydride's behavior in this condition. Hence, the sample reservoir that contains the hydrogenated alloy will be opened safely, and the events will be monitored for 6 hours.

## **8. Conclusions**

A tank for solid-state hydrogen storage was successfully designed. The selected alloy was  $(\text{TiVNb})_{67}\text{Cr}_{33}$ , which presents a plateau pressure of 0.60 bar at 15°C and 1.17 bar at 25°C, as obtained by the thermodynamic model applied. Hence, the tank pressure will not surpass 1.45 bar, as the ESS application requires. Subsequently, the hydride's mass required to store the equivalent of 5 liters of hydrogen pressurized at 150 bar was calculated based on the estimated reversible capacity of the  $(\text{TiVNb})_{67}\text{Cr}_{33}\text{H}_x$  hydride and considering a factor of safety of 50%, resulting in 3.822 kg of  $(\text{TiVNb})_{67}\text{Cr}_{33}\text{H}_x$ , that corresponds to a volume of 768 cm<sup>3</sup>. Thus, the alloy's mass required to fill the sample cylinders is 3.70 kg.

Then, two projects were done with selected Swagelok components, one having two cylinders of 500cm<sup>3</sup> (project A), and the other one having five cylinders of 150 cm<sup>3</sup> (project B). As seen in the cost projection, projects A and B's components' total costs are R\$19,394.91 and R\$38,743.66, respectively. Hence, project B is significantly the most expensive but provides better control of the hydrogen absorption process. In addition, for the  $(\text{TiVNb})_{67}\text{Cr}_{33}$  production, the total cost of the raw materials was R\$28,919.04, not counting shipping charges and the ICMS tax.

Besides, once some crucial properties can be evaluated only experimentally, a prototype and proof-of-concept tests were proposed, such as PCT measurement, H<sub>2</sub> flow evaluation, and the observation of the hydride safety in air contact. These

experiments will provide valuable information for the tank application in the future and for the project enhancement.

## 9. References

- [1] ESS, European Spallation Source, (2021). <https://europeanspallationsource.se/> (accessed July 6, 2021).
- [2] G.G. Libowitz, Metallic hydrides; fundamental properties and applications, *J. Phys. Chem. Solids.* 55 (1994) 1461–1470. [https://doi.org/10.1016/0022-3697\(94\)90571-1](https://doi.org/10.1016/0022-3697(94)90571-1).
- [3] A. Züttel, Materials for hydrogen storage, *Mater. Today.* 6 (2003) 24–33. [https://doi.org/10.1016/S1369-7021\(03\)00922-2](https://doi.org/10.1016/S1369-7021(03)00922-2).
- [4] M. Fichtner, *Nanoscale materials for hydrogen and energy storage*, Elsevier Ltd, 2009. <https://doi.org/10.1016/B978-0-08-044965-4.50009-2>.
- [5] Q. Lai, Y. Sun, T. Wang, P. Modi, C. Cazorla, U.B. Demirci, J.R. Ares Fernandez, F. Leardini, K.F. Aguey-Zinsou, How to Design Hydrogen Storage Materials? Fundamentals, Synthesis, and Storage Tanks, *Adv. Sustain. Syst.* 3 (2019) 1–64. <https://doi.org/10.1002/adsu.201900043>.
- [6] B.H. Silva, C. Zlotea, Y. Champion, W.J. Botta, G. Zepon, Design of TiVNb-(Cr, Ni or Co) multicomponent alloys with the same valence electron concentration for hydrogen storage, *J. Alloys Compd.* 865 (2021) 158767. <https://doi.org/10.1016/j.jallcom.2021.158767>.
- [7] R.B. Strozi, D.R. Leiva, G. Zepon, W.J. Botta, J. Huot, Effects of the chromium content in (TiVnb)100-xcrx body-centered cubic high entropy alloys designed for hydrogen storage applications, *Energies.* 14 (2021). <https://doi.org/10.3390/en14113068>.
- [8] G. Zepon, B.H. Silva, C. Zlotea, W.J. Botta, Y. Champion, Thermodynamic modelling of hydrogen-multicomponent alloy systems: Calculating pressure-composition-temperature diagrams, *Acta Mater.* 215 (2021) 117070. <https://doi.org/10.1016/j.actamat.2021.117070>.
- [9] BAY an NA. Olien, tables of industrial Gas - Relation Gas/Metal NBS Technical Note 1079, (1985) 200.
- [10] C. Zlotea, M.A. Sow, G. Ek, J.P. Couzinié, L. Perrière, I. Guillot, J. Bourgon, K.T. Møller, T.R. Jensen, E. Akiba, M. Sahlberg, Hydrogen sorption in TiZrNbHfTa high entropy alloy, *J. Alloys Compd.* 775 (2019) 667–674. <https://doi.org/10.1016/j.jallcom.2018.10.108>.
- [11] K. Asano, S. Hayashi, Y. Nakamura, E. Akiba, Effect of substitutional Cr on hydrogen diffusion and thermal stability for the BCT monohydride phase of the V-H system studied by <sup>1</sup>H NMR, *J. Alloys Compd.* 524 (2012) 63–68. <https://doi.org/10.1016/j.jallcom.2012.01.137>.
- [12] C.C. Shen, H.C. Li, Cyclic hydrogenation stability of  $\gamma$ -hydrides for Ti<sub>25</sub>V<sub>35</sub>Cr<sub>40</sub>

- alloys doped with carbon, *J. Alloys Compd.* 648 (2015) 534–539. <https://doi.org/10.1016/j.jallcom.2015.07.021>.
- [13] WDK. Yet-Ming Chiang, Dunbar P. Birnie, *Physical ceramics: principles for ceramic science and engineering*, *Choice Rev. Online.* 34 (1996) 34-1566-34–1566. <https://doi.org/10.5860/choice.34-1566>.
- [14] Swagelok, *Stainless Steel Seamless Tubing and Tube Support Systems catalog*, (n.d.) 1–8.
- [15] K. Young, M.A. Fetcenko, T. Ouchi, J. Im, S.R. Ovshinsky, F. Li, M. Reinhout, S. Township, *Hydrogen Storage Materials Having Excellent Kinetics, Capacity, and Cycle Stability*, 2 (2008).
- [16] S. Selvaraj, A. Jain, S. Kumar, T. Zhang, S. Isobe, H. Miyaoka, Y. Kojima, T. Ichikawa, *Study of cyclic performance of V-Ti-Cr alloys employed for hydrogen compressor*, *Int. J. Hydrogen Energy.* 43 (2018) 2881–2889. <https://doi.org/10.1016/j.ijhydene.2017.12.159>.
- [17] H.C. Lin, K.M. Lin, K.C. Wu, H.H. Hsiung, H.K. Tsai, *Cyclic hydrogen absorption-desorption characteristics of TiCrV and Ti<sub>0.8</sub>Cr<sub>1.2</sub>V alloys*, *Int. J. Hydrogen Energy.* 32 (2007) 4966–4972. <https://doi.org/10.1016/j.ijhydene.2007.07.057>.
- [18] P.D. Goodell, *Stability of rechargeable hydriding alloys during extended cycling*, *J. Less-Common Met.* 99 (1984) 1–14. [https://doi.org/10.1016/0022-5088\(84\)90330-8](https://doi.org/10.1016/0022-5088(84)90330-8).
- [19] P. Dantzer, *Metal-Hydride technology: A critical review*, *Hydrog. Met. III.* 73 (2007) 279–340. <https://doi.org/10.1007/bfb0103405>.